International Journal of Multiphysics
Volume 18, No. 2, 2024
ISSN: 1750-9548

# Hydrodynamic Characteristics of a Curved Fluid Layer with Two Porous Boundaries

**Gérémino Ella Eny[1], Gabriel Kaldjob Pom[2], Honorine Angue Mintsa Eya[1], Fils Raymond Patrick Lehel[2],**

[1]University of Sciences and Technologies of Masuku, P.O. Box 941, Franceville, Gabon
[2]University of Yaoundé I, P.O. Box 812, Yaoundé, Cameroon
Corresponding author ellaenyg@yahoo.fr

**Abstract**

This work aims to investigate the characteristics of a suction-driven flow of a curved fluid layer using the Navier-Stokes equations. The examined fluid flow characteristics include the azimuthal velocity, the normal velocity, pressure gradients, and streamlines under different values of the Reynolds number. The results show that the problem provides symmetric solutions when the fluid keeps its primary direction of motion near the two porous boundaries of the thin fluid layer. The asymmetric solutions found highlight flow reversal near each porous boundary. The change of the direction of motion due to flow reversal manifests itself as a curvature of the streamlines, and in this case the normal pressure gradient presents an oscillatory behavior.

**Keywords**: Suction-driven flow, Curved fluid layer, Navier-Stokes equations, Two-point boundary value Problem, Numerical Solutions.

## 1. Introduction

The Navier-Stokes equations [1-5] constitute an open set of differential equations giving rise to a multitude of solutions, especially when they are not associated with the constraints of time and space. Many problems encountered in nature, engineering and industries arise when considering the geometric diversity of the flow domains and the possible boundary conditions. Rectangular and circular conduits are the most encountered ducts. Consequently, by focusing attention on the fluid flow within rectangular and cylindrical channels, the boundary of the flow domain can be fixed, mobile, and porous.

The movement of a fluid in a rectangular or cylindrical domain having fixed and impermeable boundaries is a Poiseuille-type flow [6-8]. More precisely, the century-old Poiseuille flow has previously been used to estimate the mean velocity of a liquid confined in a pipe by taking into account the flow rate and the constant viscosity of the fluid, as well as the pressure difference at the longitudinal ends of the pipe. In addition, the plane Couette flow [9, 10], an important flow configuration primordial in rheology, is studied between two infinitely long rectangular plates, having longitudinal motions of different velocities in order to highlight the coexistence of laminar and turbulent zones in a flow. Moreover, a Taylor Couette flow [11, 12] is obtained by inserting a fluid between two coaxial cylinders having dissimilar rotational angular speeds such that the viscosity enables the transfer of momentum between adjacent fluid layers thus setting in motion the fluid domain, owing to cylinder walls rotation in contact with the sample fluid. Further, other types of interesting phenomena are observed when the flow boundaries are porous. Therefore, we can have boundaries that are fixed and porous, as well as dynamic and porous. The fluid flow in channels or tubes possessing two fixed porous walls [13-18] is the subject of much attention, considering the growing number of studies relating to this topic.

In the present study, the principles of conservation of mass and momentum are used to model a fluid flow in a new geometrical configuration. It is first important to point out that the mass is conserved in a fluid flow only in the absence of a sink or a source. It follows that when the fluid flows; nothing is lost nor gained in terms of the

amount of matter. The flow is often driven by suction or injection [19-25] in the cases where the fluid moves inside a porous geometrical domain. In most of these works, the mass is assumed to be conserved primarily in the case where the amount of matter entering the flow domain is the same as that leaving it [19-25, 26]. In the second case [27], the entry of matter into the flow domain or the exit of matter from the space containing the fluid is taken into account and well described, but the mass which leaves or enters through the boundaries of the flow domain is negligible compared to the total mass of the studied fluid.

The principles of conservation of mass and momentum are used in the current study which aims to examine the motion of a viscous fluid in a particular geometry that is novel and rare in the literature. Indeed, it is the flow of a fluid layer in the form of a ring having two permeable borders where the phenomenon of suction occurs. More precisely, the suction represents the mass withdrawal during the flow process. From the geometric point of view, the flow consists of a linear velocity of rotation also known as the azimuthal velocity deduced from the circular movement of the fluid and a normal velocity which results from the phenomenon of suction that takes place across the porous borders of the flow domain. Ultimately, the analysis of the fluid motion is based on determining the flow field components that directly intervene in the fundamental relationship of dynamics, notably the velocity and the pressure gradient. In addition, mindful of the steadiness of the flow, the streamlines representing the trajectories for the steady flow under study are plotted in order to better understand the displacement of fluid particles in the flow field.

## 2. Model Equations

A cylindrical polar coordinate system ($r^*$, $\theta$, $z^*$) is used to model a thin fluid layer in a curved motion induced by suction as shown in Fig. 1.

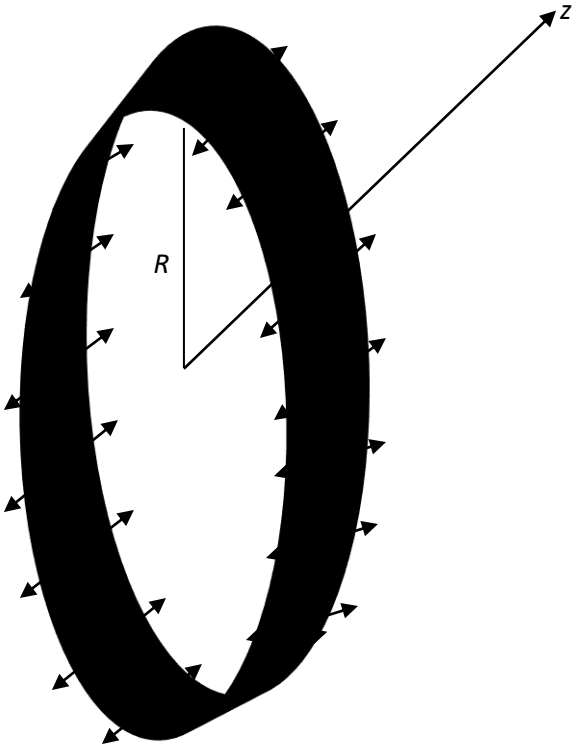


Figure 1: Sketch of the curved thin fluid layer with seepage at the two porous boundaries

The velocity field consists of the linear velocity of rotation $u^*$ and the normal or the axial component $w^*$. On the other hand, the variable describing the pressure in the flow field is $p^*$. Due to the thinness of the fluid layer; gravity terms do not influence the flow under study. The flow is driven by suction such that $V$ represents the absolute fluid withdrawal speed at the two porous boundaries situated at $z^* = -a$ and $z^* = a$, respectively.

Consequently, $a$ denotes the half-width of the flow field such that $2a$ is the total distance between the two permeable borders. The physical properties of the working fluid are considered constant, notably the specific mass $\rho$ and the kinematic viscosity $\nu$. It follows that, in the current geometry, the equations of motion of the incompressible viscous fluid are given by:

$$\frac{1}{R^*}\frac{\partial u^*}{\partial \theta}+\frac{\partial w^*}{\partial z^*}=0 \tag{1}$$

$$\frac{u^*}{R^*}\frac{\partial u^*}{\partial \theta}+w^*\frac{\partial u^*}{\partial z^*}=-\frac{1}{\rho}\frac{1}{R^*}\frac{\partial p^*}{\partial \theta}+\nu\left(\frac{1}{R^{*2}}\frac{\partial^2 u^*}{\partial \theta^2}+\frac{\partial^2 u^*}{\partial z^{*2}}-\frac{u^*}{R^{*2}}\right) \tag{2}$$

$$\frac{u^*}{R^*}\frac{\partial w^*}{\partial \theta}+w^*\frac{\partial w^*}{\partial z^*}=-\frac{1}{\rho}\frac{\partial p^*}{\partial z^*}+\nu\left(\frac{1}{R^{*2}}\frac{\partial^2 w^*}{\partial \theta^2}+\frac{\partial^2 w^*}{\partial z^{*2}}\right) \tag{3}$$

where the continuity Eq. (1) describes mass conservation owing to the fact that the suction phenomenon is considered and described, but the quantity of matter extracted when the flow occurs is negligible compared to the total mass of the fluid inside the flow domain. On the other hand, the momentum conservation is expressed by the Navier-Stokes Eqs. (2) and (3). It appears that these equations are written in an unusual manner, as the radial coordinate $r^* = R^*$ is assumed to be constant, because of the thinness of the curved fluid layer. The boundary conditions are given by:

$$\begin{aligned} &u^* = 0, w^* = -V \quad \text{for} \quad z^* = -a \\ &u^* = 0, w^* = V \quad \text{for} \quad z^* = +a \end{aligned} \tag{4}$$

More precisely, the boundary conditions $u^* = 0$ for $z^* = \pm a$, express the no-slip condition where we have enforced that the two flow borders are fixed. In addition, the boundary conditions $w^* = \pm V$ derive from equal suction flow rates at boundaries.

As the reference data of the problem are presented, it is relevant at this stage to state the problem in a nondimensional formulation enabling the control numbers that govern the dynamics of the fluid under study to be highlighted. To reach this objective, using the scale provided by the geometry of the flow domain, the lengths are normalized by the half-width $a$ of the fluid layer as follows:

$$r = R = \frac{R^*}{a}, \qquad z = \frac{z^*}{a} \tag{5}$$

Moreover, the linear velocity of rotation and the normal velocity can be measured in units of the absolute suction speed at boundaries $V$ in light of the formulas:

$$u = \frac{u^*}{V}, \qquad w = \frac{w^*}{V} \tag{6}$$

Finally, the reference pressure $(\rho V^2)$ is used to normalize the pressure within the flow field as in the following:

$$p = \frac{p^*}{\rho V^2} \tag{7}$$

By considering Eqs. (5)-(7), the nondimensional differential equations of the problem are derived:

$$\frac{1}{R}\frac{\partial u}{\partial \theta}+\frac{\partial w}{\partial z}=0 \tag{8}$$

$$\frac{u}{R}\frac{\partial u}{\partial \theta}+w\frac{\partial u}{\partial z}=-\frac{1}{R}\frac{\partial p}{\partial \theta}+\frac{1}{\mathrm{Re}}\left(\frac{1}{R^2}\frac{\partial^2 u}{\partial \theta^2}+\frac{\partial^2 u}{\partial z^2}-\frac{u}{R^2}\right) \tag{9}$$

$$\frac{u}{R}\frac{\partial w}{\partial \theta}+w\frac{\partial w}{\partial z}=-\frac{\partial p}{\partial z}+\frac{1}{\mathrm{Re}}\left(\frac{1}{R^2}\frac{\partial^2 w}{\partial \theta^2}+\frac{\partial^2 w}{\partial z^2}\right) \tag{10}$$

where the Reynolds number Re = $aV/\nu$ is derived. The nondimensional Eqs. (8)-(10) are associated with the following boundary conditions:

$u = 0,$ $w = -1$ for $z = -1$

$u = 0,$ $w = 1$ for $z = +1$ (11)

The governing equations show that the flow is described by two velocity components. Upon closely examining Eqs. (8)-(10), we determine that the system can be solved by defining and introducing a stream function $\psi$ related to velocity components as follows:

$$u=\frac{\partial \psi}{\partial z}, \qquad w=-\frac{1}{R}\frac{\partial \psi}{\partial \theta} \tag{12}$$

Consequently, using the stream function as defined in Eq. 12, ensures that Eq. (8) is self-satisfied. It follows that the introduction of the stream function in the governing equations is a shortcut since it enables a transformation from three differential Eqs. (8)-(10) to only a single differential equation governing the lone dependent variable, the stream function, for the same problem. In fact, by taking the curl of the vector form of the two Navier-Stokes Eqs. (9) and (10), the vorticity equation satisfied by the stream function is obtained and given by:

$$\frac{1}{R}\left(\frac{\partial \psi}{\partial \theta}\frac{\partial}{\partial z}\left(D^2\psi\right)-\frac{\partial \psi}{\partial z}\frac{\partial}{\partial \theta}\left(D^2\psi\right)\right)=-\frac{1}{\mathrm{Re}}D^4\psi+\frac{1}{\mathrm{Re}}\frac{1}{R^2}\frac{\partial^2 \psi}{\partial z^2} \tag{13}$$

where $D^2\psi=\frac{1}{R^2}\frac{\partial^2 \psi}{\partial \theta^2}+\frac{\partial^2 \psi}{\partial z^2}$. The solution of the non-linear partial differential equation Eq. (13) is determined by imposing the following boundary conditions:

$$\frac{\partial \psi}{\partial z}=0, \qquad \frac{1}{R}\frac{\partial \psi}{\partial \theta}=1 \qquad \text{for } z=-1$$

$$\frac{\partial \psi}{\partial z}=0, \qquad \frac{1}{R}\frac{\partial \psi}{\partial \theta}=-1 \qquad \text{for } z=+1 \tag{14}$$

As the flow is a steady one, the mass transfer per unit length of the circumference of the thin fluid layer is useful and a similarity transformation is also derived:

$$\psi(\theta,z)=\eta F(z) \tag{15}$$

where $\eta=R\theta$ denotes a variable derived from the curved form of the thin fluid layer. By considering Eq. (15), the final form of the equation governing the problem to solve is obtained as follows:

$$F^{(4)}-\frac{1}{R^2}F^{(2)}+\mathrm{Re}(FF^{(3)}-F^{(1)}F^{(2)})=0 \tag{16}$$

where $F^{(i)}=d^{(i)}F/dz^{(i)}$. Further, due to the transformation (15), the boundary conditions of the problem become:

$$F(-1) = 1, \qquad F^{(1)}(-1) = 0$$
$$F(1) = -1, \qquad F^{(1)}(1) = 0 \tag{17}$$

It is interesting to note that Eq. (16) associated with the boundary conditions (17) represent a two-point boundary-value problem which differs in form from the well-known previous mathematical formulation of a two-dimensional flow in a channel with two fixed porous walls [28, 29]. This difference is due to the presence of the term $-\frac{1}{R^2}F^{(2)}$ of Eq. (16) related to the curved form of the flow domain. In fact, the nondimensional radius of the curved fluid layer $R$ is a measure of the aspect ratio that expresses the comparison between the dimensional radius $R^*$ and the half-width $a$ of the curved flow domain. In other words, the nondimensional geometric parameter $R$ is also the ratio between the diameter of the thin curved fluid layer $2R^*$ and the total width $2a$ of the flow field.

The expressions of the nondimensional azimuthal velocity $u$ and the normal velocity $w$ in terms of function $F$ are deduced from Eqs. (12) and (15) such that:

$$u = \eta F^{(1)}(z), \qquad w = -F(z) \tag{18}$$

On the other hand, the azimuthal pressure gradient per unit length of the circumference of the curved fluid layer is defined by:

$$\frac{1}{\eta}\frac{\partial p}{\partial \eta} = \frac{1}{\mathrm{Re}}\left( F^{(3)} - \frac{F^{(1)}}{R^2} + \mathrm{Re}\left(FF^{(2)} - (F^{(1)})^2\right)\right) \tag{19}$$

In light of Eq. (19), at a given Reynolds number Re, the azimuthal pressure gradient per unit length of the circumference of the flow field is constant, since it is equivalent to the integral of the fluid distribution Eq. (16). On the other hand, the normal pressure gradient is derived from the formula:

$$\frac{\partial p}{\partial z} = -\frac{1}{\mathrm{Re}}F^{(2)} - FF^{(1)} \tag{20}$$

It is relevant to note that the normal pressure gradient as defined in Eq. (20) plays an important role in this investigation and deserves much attention because it governs the withdrawal process of the fluid as the flow under study is induced by suction.

## 3. Results and Discussions

The numerical results in terms of the stream function per unit length of the circumference of the flow field $F$ are obtained by solving the two-point boundary-value problem (16)-(17) using the shooting method associated with a fourth-order Runge-Kutta scheme [30]. Then the flow characteristics in terms of velocity components, pressure gradients, and streamlines are determined by using their respective relationships with function $F$ and its derivatives. These flow characteristics are eventually determined as symmetric and asymmetric solutions. More precisely, the analysis is focalized on three kinds of symmetric solutions and two kinds of asymmetric solutions that are highlighted by increasing the Reynolds number in the case where the width of the flow domain and the diameter of the curved fluid layer are of equal importance, such that $R$ =1.

### 3.1. PROFILES OF THE AZIMUTHAL VELOCITY

The azimuthal velocity per unit length of the circumference of the curved fluid layer is presented in Figs. 2-6. In particular, the symmetric solutions of the first kind that exist for low and high values of the Reynolds number as shown in Fig. 2 present parabolic curves resulting from the fact that the flow keeps its primary direction of motion, that is the direction derived from the boundary conditions of the problem at low values of the Reynolds number. However, the curves of Fig. 2 become flat when the Reynolds number increases due to the appearance of a boundary layer type flow which manifests itself as a same constant profile for different high values of Re.

In other words, from low to high values of the Reynolds number relative to the symmetric solutions of the first kind, the dynamics of the fluid begins with a creeping type flow to a boundary layer type flow, respectively; such that the function $u/\eta$ increases with Re in the neighborhood of the middle region of the flow, while a decrease occurs near the boundaries. More precisely, the middle region of the flow is the central circle of the thin curved fluid layer. As the Reynolds number increases above the value of 6.413, the symmetric solutions of the first kind persist, but two new asymmetric solutions of the first and second kinds which are respectively depicted in Figs. 3 and 4 also arise.

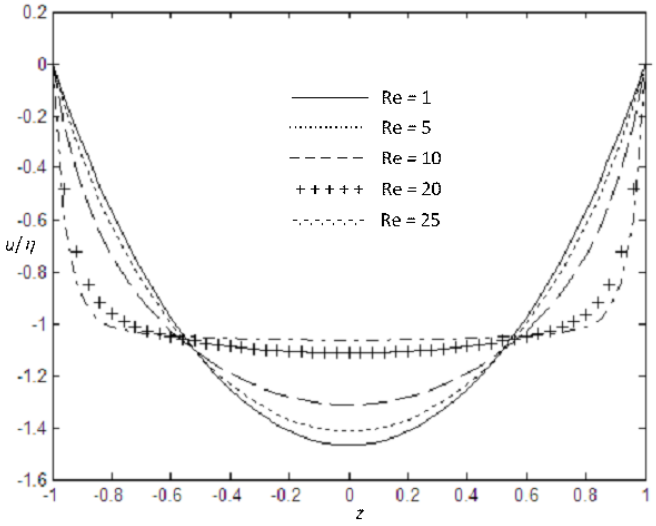


Figure 2: Linear velocity of rotation per unit length of the circumference relative to symmetric solutions of the first kind

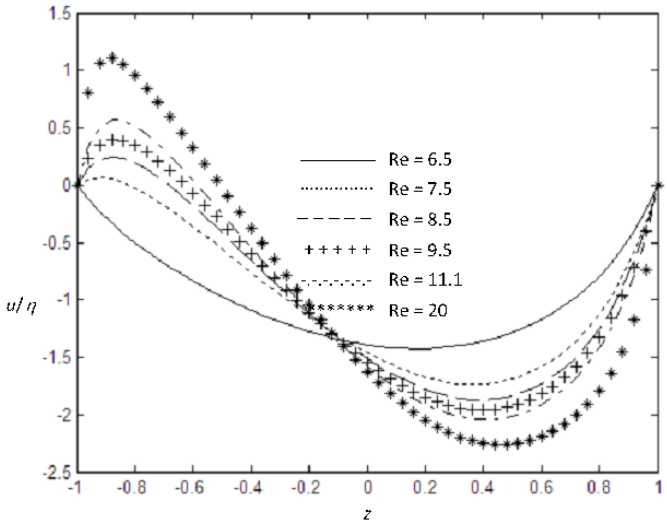


Figure 3: Linear velocity of rotation per unit length of the circumference relative to asymmetric solutions of the first kind

It appears that the asymmetric flow prevents the manifestation of the boundary layer, but the backward motion takes place near the boundaries, with the difference that, this backward motion also known as flow reversal occurs in the neighborhood of the border $z = -1$ relative to the asymmetric solutions of the first kind plotted in Fig. 3. On the other hand, from Fig. 4, it is seen that flow reversal moves from the vicinity of the border $z = -1$ to the neighborhood of the boundary $z = 1$ with respect to the asymmetric solutions of the second kind. It is relevant in this study to note that, for the primary direction of motion, the flow velocity is such that $u < 0$, and flow reversal occurs when $u > 0$. The dynamics of the fluid exhibited in Figs. 3 and 4 leads to the conclusion that the asymmetric solutions of the first and second kinds behave as mirror images of each other. More

precisely, the backward flow occurs when the fluid moves in the opposite direction to the primary motion as the Reynolds number increases. This growth of the Reynolds number increases the linear velocity of rotation per unit length of the circumference near the border $z$ = -1, but decreases this velocity in the neighborhood of the border z = 1 relative to the asymmetric solutions of the first kind as plotted in Fig. 3. On the other hand, the linear velocity of rotation per unit length of the circumference corresponding to the asymmetric solutions of the second kind decreases with the increasing Reynolds number close to the boundary $z$ = -1, while an increase is observed near the boundary $z$ = 1.

As the Reynolds number grows above the value of 12.614, the symmetric solutions of the first kind and the asymmetric solutions persist, but two new symmetric solutions appear, that is the symmetric solutions of the second and third kinds as shown in Figs. 5 and 6, respectively. As the flow reverses near one border with respect to each asymmetric solution; about the symmetric solutions of the second kind, this flow reversal moves from the borders to the middle domain of the flow in light of Fig. 5 which presents positive values for function $u/\eta$ around the region $z$ = 0. For added clarity, the data obtained from the numerical integration show that the backward flow develops near the middle region of the flow relative to the symmetric solutions of the second kind if the Reynolds number satisfies Re < 13.828. However, the values of the Reynolds number superior to 13.828 destroy the reverse flow as illustrated by Fig. 5. On the other hand, the fluid motion is totally reversed near the middle area of the flow field for all the values of the Reynolds number with respect to symmetric solutions of the third kind according to Fig. 6 which also shows that the linear velocity of rotation per unit length of the circumference increases with the Reynolds number near the middle region of the thin fluid layer, but decreases close to the porous boundaries.

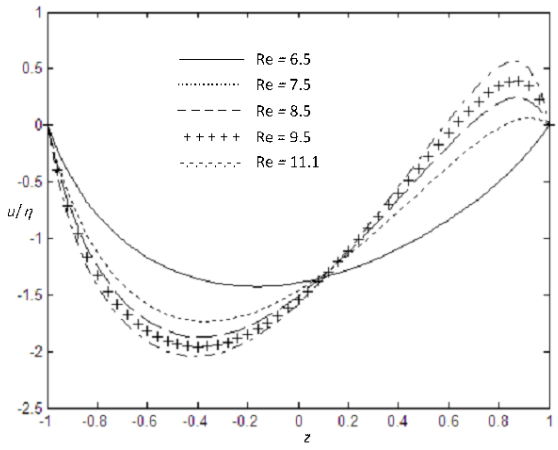


Figure 4: Linear velocity of rotation per unit length of the circumference relative to asymmetric solutions of the second kind

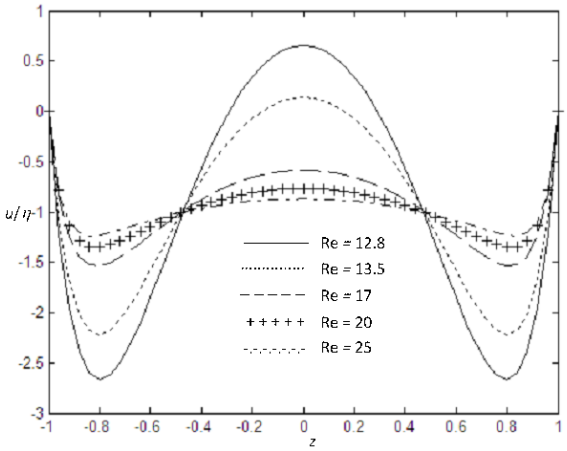


Figure 5: Linear velocity of rotation per unit length of the circumference corresponding to symmetric

solutions of the second kind

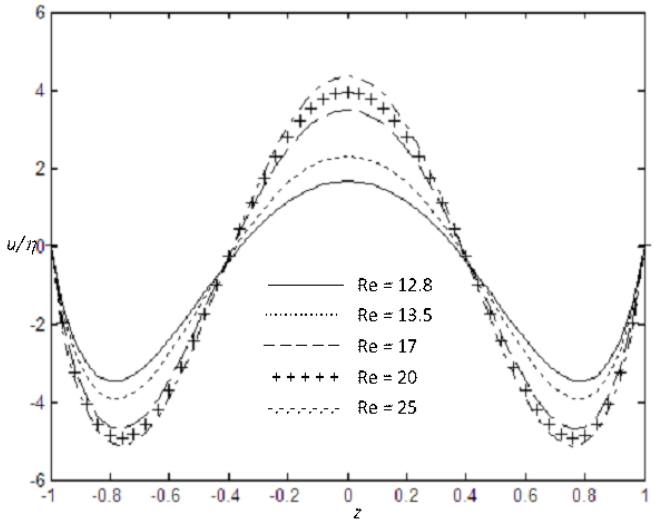


Figure 6: Linear velocity of rotation per unit length of the circumference corresponding to symmetric solutions of the third kind

## 3.2. PROFILES OF THE NORMAL VELOCITY

The normal velocity presented in Figs. 7-11 vanishes in the middle of the flow domain due to the symmetry highlighted in the problem under study, precisely for the symmetric solutions of the first, second and third kinds as shown in Figs. 7, 10 and 11; with the difference that the profiles of function $w$ tend to satisfy a linear law of the form $w = z$ [31, 32] by increasing the Reynolds number because of the development of the boundary layer by focusing the attention on Fig. 7. The advent of the asymmetric solutions causes the magnitude of the normal velocity to exceed its value established at boundaries, especially when the Reynolds number increases according to Figs. 8 and 9. More precisely, these values of the normal velocity exceeding its magnitude at boundaries are located near the border $z = -1$with respect to the asymmetric solutions of the first kind, and close to the border $z = 1$ relative to the asymmetric solutions of the second kind. Indeed, the normal velocity overshoots due to flow reversal that is highlighted through the asymmetric solutions. The behavior of the normal velocity within the flow domain as a function of Re is well depicted by referring to Figs. 8 and 9, such that with the growth of the Reynolds number, it decreases in Fig. 8 about the asymmetric solutions of the first kind, while it increases in Fig. 9 concerning the asymmetric solutions of the second kind.

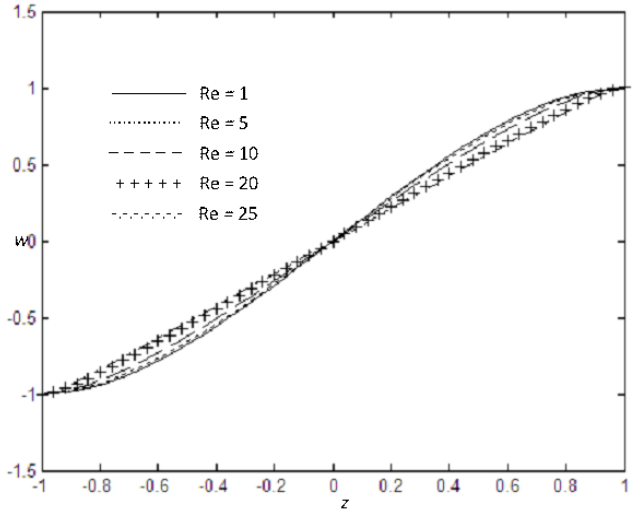


Figure 7: Normal velocity related to symmetric solutions of the first kind

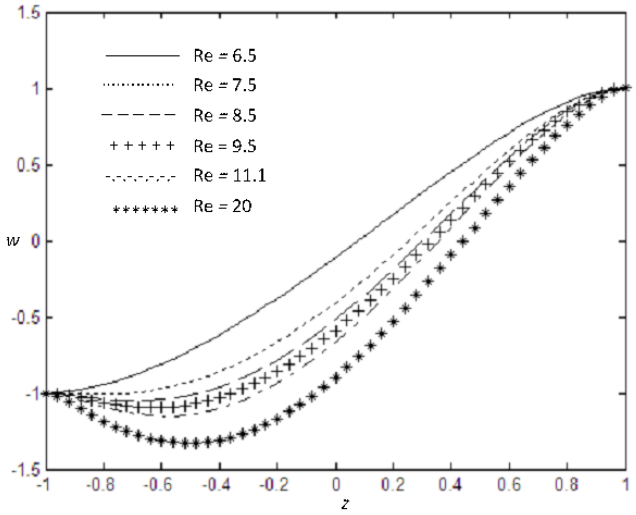


Figure 8: Normal velocity related to asymmetric solutions of the first kind

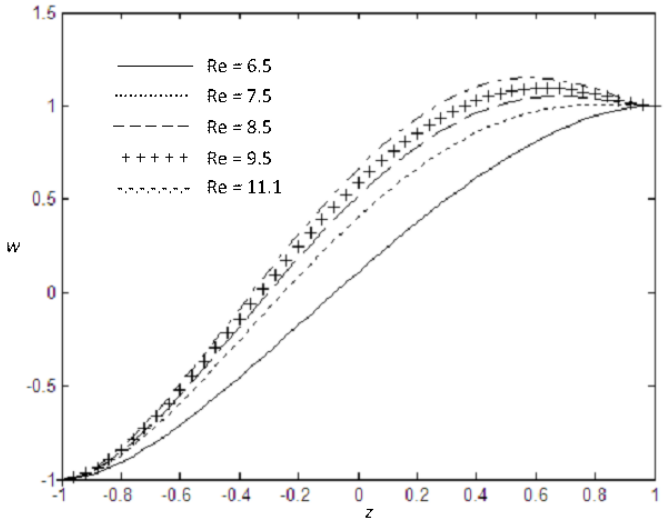


Figure 9: Normal velocity related to asymmetric solutions of the second kind

The curves of Fig. 10 exhibit an inflection highlighting flow reversal in the middle region of the flow for Re < 13.828 relative to symmetric solutions of the second kind, while other curves in the same figure obtained for Re > 13.828 show the disappearance of the inflection. The coexistence of flow reversal in the middle domain of the flow field and the primary direction of motion near the boundaries involves the oscillatory profile of the normal velocity pertaining to the symmetric solutions of the third kind plotted in Fig. 11. Among the hydrodynamic structures revealed in this work, it appears that the symmetric solutions of the second kind represent a flow regime where the increase in Reynolds number is more favorable to the development of the flow following the primary direction of motion around the middle domain of the fluid layer. However, concerning the symmetric solutions of the first kind, the growth in Reynolds number tends to oppose the maintenance of the primary direction of motion around the middle region of the flow field, although the azimuthal velocity remains negative everywhere inside the space occupied by the fluid. On the other hand, the total disappearance of the primary direction of motion near the central circle of the curved fluid layer is met in the case of symmetric solutions of the third kind.

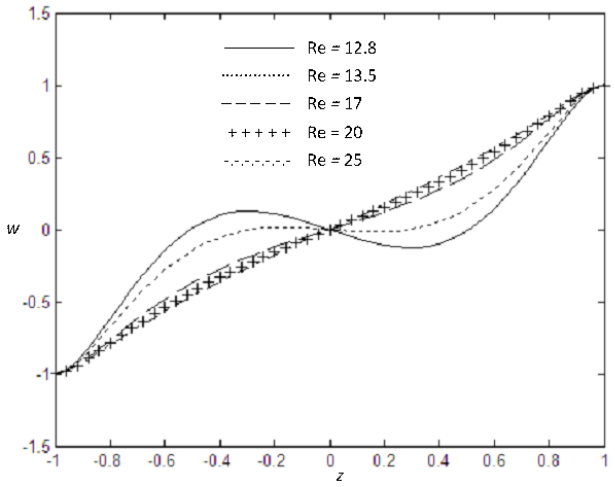


Figure 10: Normal velocity corresponding to symmetric solutions of the second kind

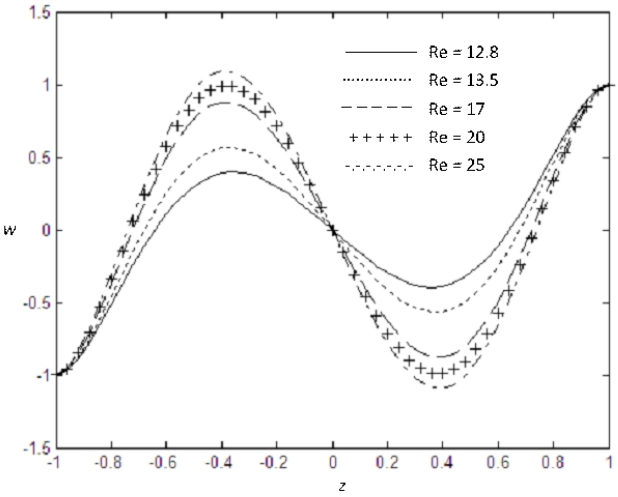


Figure 11: Normal velocity corresponding to symmetric solutions of the third kind

### 3.3. PRESSURE GRADIENT

As the flow regime pertaining to symmetric solutions of the first kind reveals an important suction flux for a low Reynolds number, the normal pressure gradient presents large variations inside the flow field compared to its variations corresponding to high values of the control parameter Re in light of Fig. 12. Indeed, the growth of the Reynolds number tends to reduce the magnitude of the suction at boundaries; that is why the corresponding values of the normal pressure gradients do not show enough difference and seem to be presented as a same constant curve. Indeed, the phenomenon of the normal pressure gradients plotted under different high Reynolds numbers tending to a same constant curve is due to the boundary layer. On the other hand, as the flow occurs by changing the direction near the boundaries, the normal pressure gradient presents large variations through the asymmetric solutions plotted in Figs. 13 and 14. Due to the symmetry, Fig. 12 shows that the normal pressure gradient vanishes for all the Reynolds numbers in the middle region of the flow field known as the central circle of the thin fluid layer, while this pressure gradient presents its maxima and its minima near the middle region of the fluid layer relative to asymmetric solutions of the first and second kinds, especially for high values of the Reynolds number by referring to Figs. 13 and 14, respectively. Indeed, the large positive and negative normal pressure gradients obtained near the central circle of the curved fluid layer are in accordance with the behavior of the normal velocity component that overshoots by exceeding its magnitude at boundaries. Around the central circle of the curved fluid layer, the described maxima are great as the Reynolds number increases according to asymmetric solutions of the first kind; on the other hand, the minima are low as the Reynolds number increases about the asymmetric solutions of the second kind. However, the asymmetric solution kind that admits a

maximum in terms of the normal pressure gradient near the central circle of the curved fluid layer provides a minimum corresponding to the same value of the Reynolds number close to the border $z = 1$. Moreover, the asymmetric solution kind that exhibits a minimum in terms of the normal pressure gradient around the central circle of the curved fluid layer presents a maximum corresponding to the same value of the Reynolds number close to the border $z = -1$.

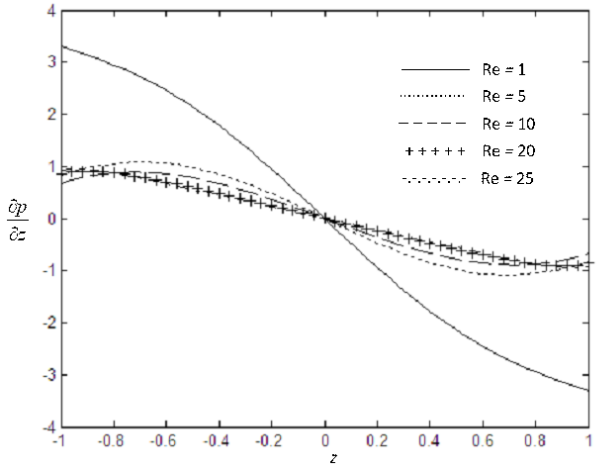


Figure 12: Normal pressure gradient relative to symmetric solutions of the first kind

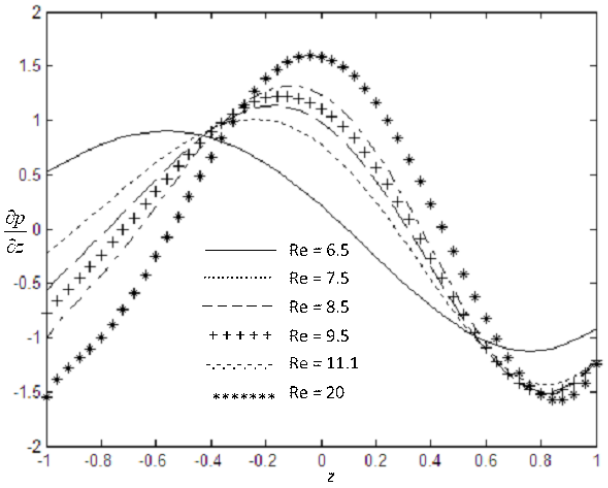


Figure 13: Normal pressure gradient relative to asymmetric solutions of the first kind

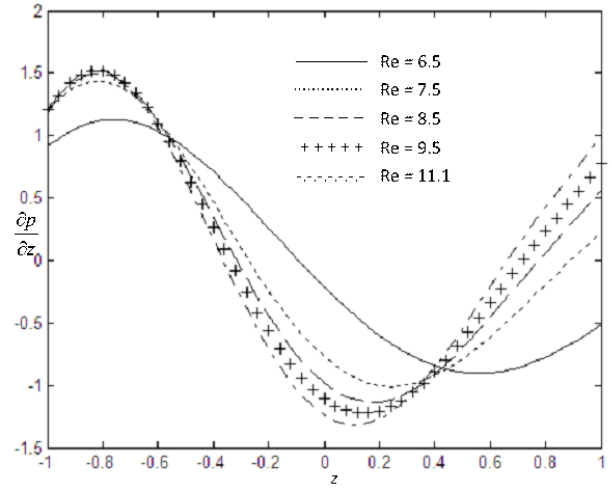

Figure 14: Normal pressure gradient relative to asymmetric solutions of the second kind

The normal pressure gradient decreases inside the flow field from the border $z = -1$ to the border $z = 1$ for each value of the Reynolds number according to the symmetric solutions of the second kind presented in Fig. 15 which shows two types of curves, notably those which correspond to the values of the Reynolds number satisfying $Re < 13.828$; and those related to the Reynolds numbers satisfying $Re > 13.828$. More precisely, as the flow reverses in the case $Re < 13.828$, the normal pressure gradient presents great variations inside the flow domain, while other curves obtained for $Re > 13.828$ do not present enough variations because the flow keeps its primary direction of motion. On the other hand, the existence of the alternating regions of flow reversal and those of the flow occurring in the primary direction of motion relative to the symmetric solutions of the third kind gives rise to the oscillations of the normal pressure gradient with not constant amplitude as shown in Fig. 16.

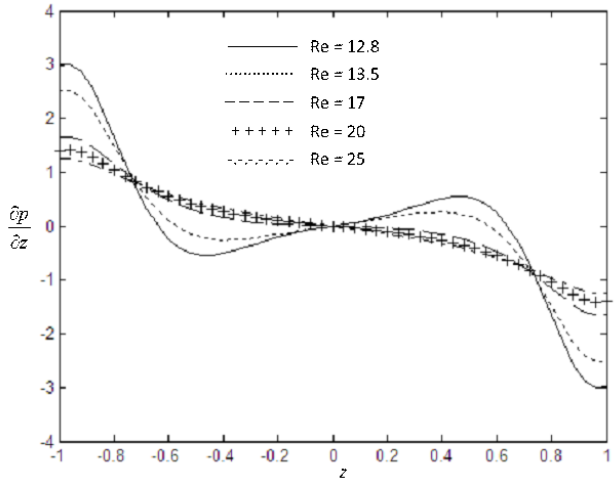


Figure 15: Normal pressure gradient relative to symmetric solutions of the second kind

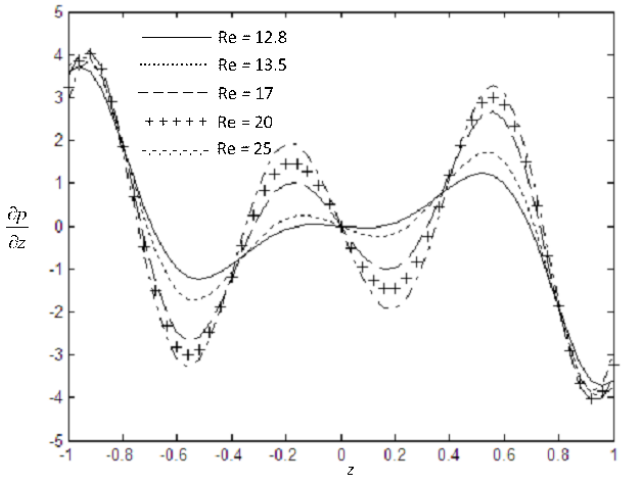


Figure 16: Normal pressure gradient relative to symmetric solutions of the third kind

3.4. STREAMLINES

Since the streamlines are tangent at any point of the flow domain to the velocity vector of the steady problem under study, they enable to apprehend the behavior of the velocity field of the fluid. The flow patterns related to symmetric solutions of the first kind highlighted in Fig. 17 show how the fluid keeps the same direction of motion from the core of the space occupied by the fluid to the porous borders where the suction process takes place. In other words, the flow process exhibited in Fig. 17 begins parallel to the central circle of the thin fluid layer and becomes orthogonal to the porous boundaries due to suction. On the other hand, the curvature of the

streamlines in Fig. 18 near the border $z$ = -1 demonstrates the development of flow reversal with respect to asymmetric solutions of the first kind, while this flow reversal moves from the boundary $z$ = -1 to the boundary $z$ = 1 about the asymmetric solutions of the second kind plotted in Fig. 19. At this stage, it is important to note that the plot of the streamlines enables to show how the fluid is equally distributed on both sides of the central circle of the flow domain concerning the symmetric solutions in Figs. 17 and 20-22, as well as how this symmetry is destroyed by the appearance of the asymmetric solutions in Figs. 18 and 19.

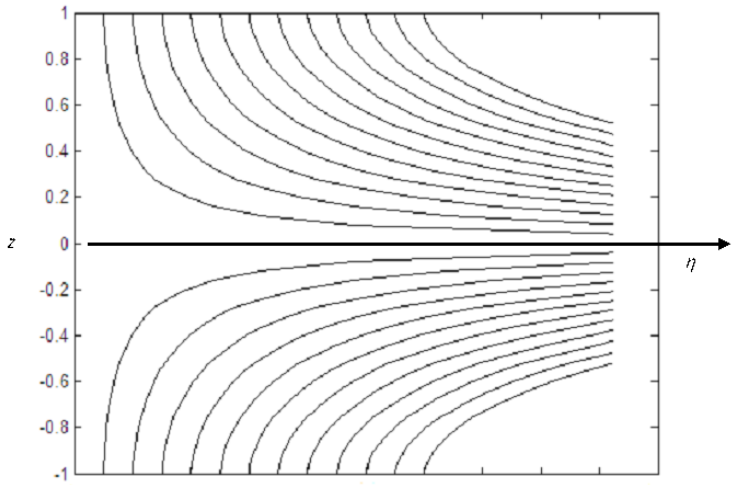


Figure 17: Top view of the flow pattern corresponding to symmetric solutions of the first kind for Re = 10

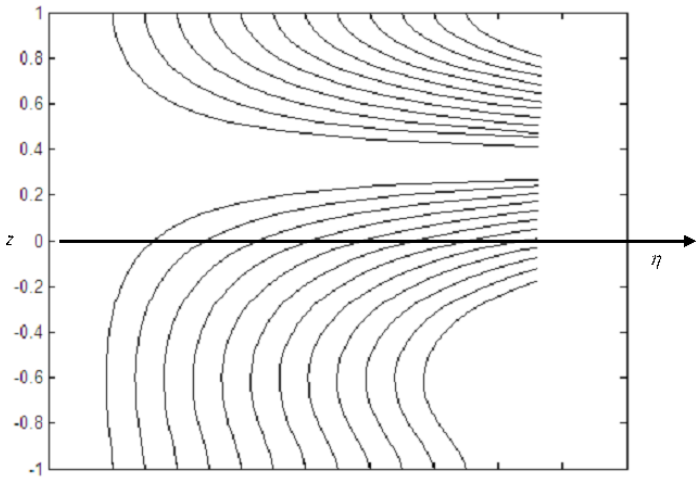


Figure 18: Top view of the flow pattern corresponding to asymmetric solutions of the first kind for Re = 10.

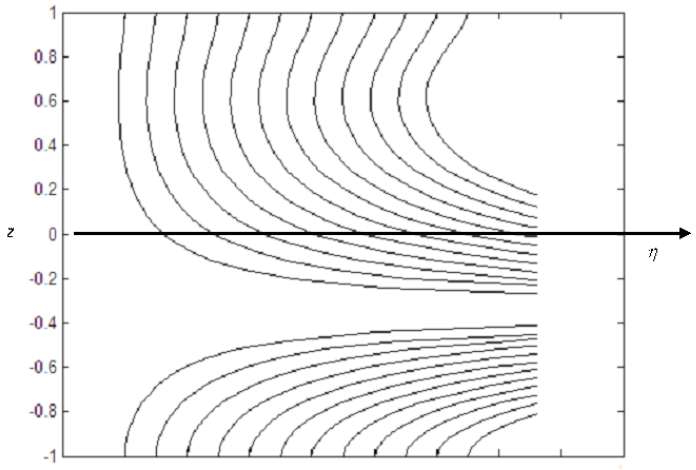


Figure 19: Top view of the flow pattern corresponding to asymmetric solutions of the second kind for Re = 10

Near the core of the space occupied by the fluid, the flow can reverse or it can move in the primary direction depending on the values of the Reynolds number, that is why Fig. 20 is devoted to presenting the curvature of the streamlines close to the middle region of the flow field for Re < 13.828 relative to symmetric solutions of the second kind. Moreover, although the flow patterns obtained in Fig. 20 are far from the borders but close to the core of the fluid layer, the streamlines reveal that the flow keeps its primary direction when the suction occurs near the borders. On the other hand, for Re > 13.828, the symmetric solutions of the second kind in the absence of flow reversal reveal the disappearance of the curvature of the streamlines in Fig. 21 which shows the same direction of motion of the whole fluid layer. Figure 21 also shows the set of streamlines close to the core of the flow domain but far from the porous borders. The behavior of the flow described in Fig. 20 for Re < 13.828 about the symmetric solutions of the second kind, is generalized for all the values of the Reynolds number concerning the streamlines achieved for symmetric solutions of the third kind through Fig. 22; with the difference that the streamlines in this last figure occupy the whole flow domain. More precisely, with respect to symmetric solutions of the third kind, the curvature of the streamlines takes place around the middle of space occupied by the fluid layer as the flow is totally reversed in this region for all the values of the main control parameter of the problem.

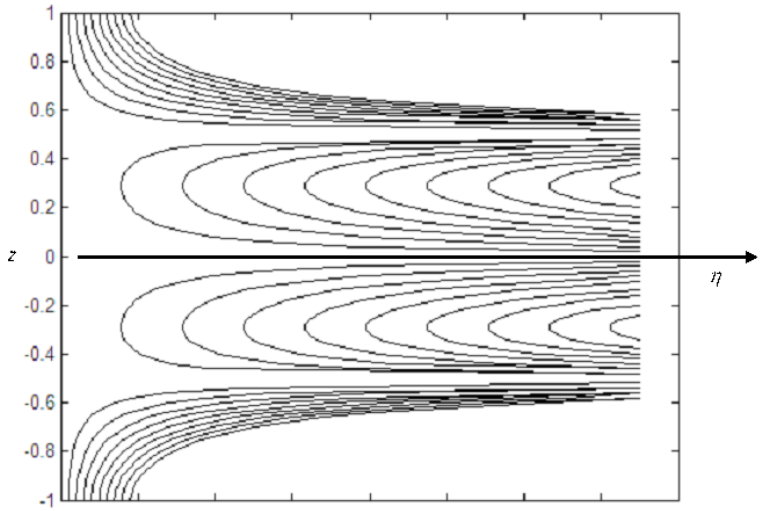


Figure 20: Top view of the flow pattern corresponding to symmetric solutions of the second kind in the case of flow reversal for Re = 12.8

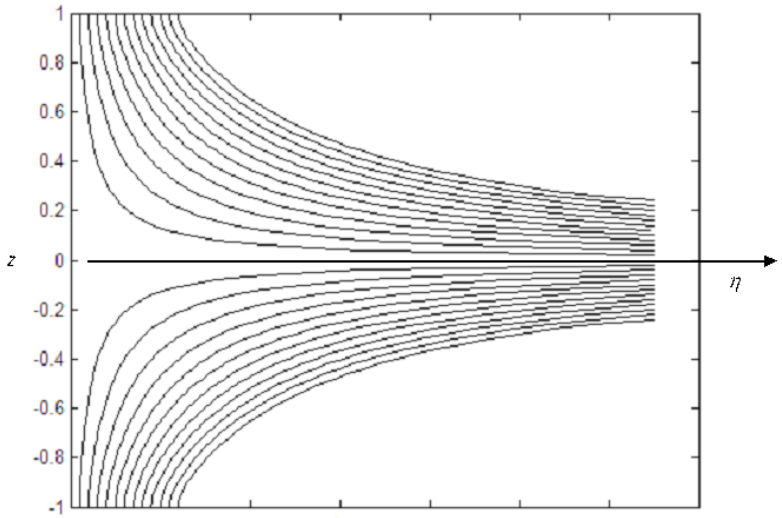


Figure 21: Top view of the flow pattern corresponding to symmetric solutions of the second kind in the absence of flow reversal for Re = 20

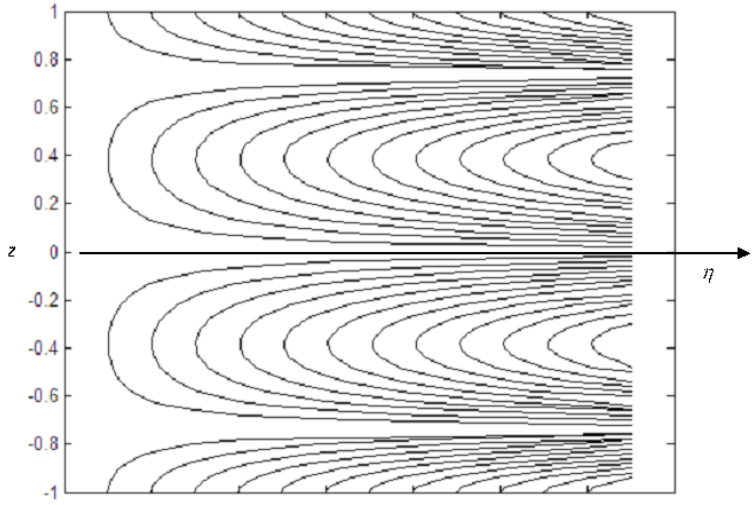


Figure 22: Top view of the flow pattern corresponding to symmetric solutions of the third kind for Re = 20

## 4. Conclusion

The azimuthal velocity per unit length of the circumference of the thin curved fluid layer increases with the Reynolds number near the middle area of the flow field relative to symmetric solutions of the first and third kinds, while it decreases with respect to symmetric solutions of the second kind. This difference in the description of the behavior of the symmetric solutions found in this study is due to the fact that, symmetric solutions of the second kind are the only solutions that reveal flow reversal around the middle of the flow domain by decreasing the Reynolds number from the value of 13.828. This behavior of the symmetric solutions of the second kind inspired the realization of two figures, notably Figs. 20 and 21 in order to properly describe the flow patterns corresponding to $Re < 13.828$ when the flow reverses and $Re > 13.828$ in the absence of the backward flow in the neighborhood of the middle area of the space occupied by the fluid layer. Moreover, the assumption that the direction of the flow near the porous boundaries remains the same for all the symmetric solutions is well exhibited by the streamlines plotted in Figs. 17, 20-22. On the other hand, as this direction of motion is not kept about the asymmetric solutions near the two porous boundaries, a curvature of the streamlines

is observed close to the border $z$ = -1 in the case of asymmetric solutions of the first kind plotted in Fig. 18, while this curvature of the streamlines moves from the border $z$ = -1 to the border $z$ = 1 in Fig. 19 highlighting the flow patterns about the asymmetric solutions of the second kind. It appears that the streamlines are equally distributed on both sides of the central circle of the fluid layer in the case of symmetric solutions, while this central circle does not divide into two equal parts the set of the streamlines corresponding to asymmetric solutions. In this work, the plots of the streamlines are used to confirm the flow structures revealed from the analysis of the behavior of the velocity components.

The interesting behavior of the pressure gradient bears a strong correlation to that of the velocity field. This can be explained by the momentum conservation which is assumed in the present study, such that the normal pressure gradient tends to undergo oscillatory variations resulting from the coexistence of flow reversal and the primary direction of motion within the space occupied by the fluid, especially concerning the symmetric solutions of the third kind.

Finally, in comparison with previous results [28, 29], the new geometry investigated in this study dealing with the porous curved fluid layer reveals quantitative changes in the hydrodynamic structures that characterize fluid flows between two porous walls due to the modification of the Navier-Stokes equations by the presence of the term $-F^{(2)}/R^2$. However, the hydrodynamic structures found in the present study do not show qualitative changes in comparison with the previous literature about fluid flows between two porous boundaries.

**Refrences**

[1] Bird, R. B., Stewart, W. E. and Lightfoot, E. N., *Transport Phenomena*, 2nd edition, Wiley, New York, 2002.
[2] Bird, R. B., Armstrong, R. C. and Hassager, O., *Dynamics of Polymeric Fluids*: *Volume 1 Fluid Mechanics*. Wiley, New York, 1987.
[3] Kays, W. M., *Convective Heat and Mass Transfer*, McGraw-Hill, New York, 1966.
[4] White, M. F., *Viscous Fluid Flow*, McGraw-Hill, New York, 1991.
[5] Reid, R. C., Prausnitz, J. M. and Poling, B. E., *The Properties of Gases and Liquids*, 4th edition, McGraw-Hill, New York, 1987.
[6] Carlson, D. R., Widnall, S. E. and Peters, M. F., A Flow-Visualizaton Study of Transition in Plane Poiseuille Flow, *Journal of Fluid Mechanics*, 1982, 121, 487-505.
[7] Nishioka, M. and Asai, M., Some Observations of the Subcritical Transition in Plane Poiseuille Flow, *Journal of Fluid Mechanics*, 1985, 150, 441-450.
[8] Schäfer, P. and Herwig, H., Stability of Plane Poiseuille Flow with Temperature Dependent Viscosity, *International Journal of Heat and Mass Transfer*, 1993, 36(6), 2441-2448.
[9] Case, K. M., Stability of Inviscid Plane Couette Flow, *Physics of Fluids*, 1960 3(2), 143-148.
[10] Coles, D., Transition in Circular Couette Flow, *Journal of Fluid Mechanics*, 1965, 21(3), 385-425.
[11] Wereley, S. T. and Lueptow, R. M., Velocity Field for Taylor-Couette Flow with an Axial Flow, *Physics of Fluids*, 1999, 11(12), 3637-3649.
[12] Donnelly, R. J., Taylor-Couette Flow: the Early Days, *Physics Today*, 1991, 44(11), 32-39.
[13] Granger, J., Dodds, J. and Midoux, N., Laminar Flow in Channels with Porous Walls, *The Chemical Engineering Journal*, 1989, 42(3), 193-204.
[14] Karode, S. K., Laminar Flow in Channels with Porous Walls, Revisited, *Journal of Membrane Science*, 2001, 191(1-2), 237-241.
[15] Kahshan, M., Lu, D. and Rahimi-Gorji, M., Hydrodynamical Study of Flow in a Permeable Channel: Application to Flat Plate Dialyzer, *International Journal of Hydrogen Energy*, 2019, 44(31), 17041-17047.
[16] Siddiqui, A. M. and Azim, Q. A., Creeping Flow of a Viscous Fluid in a Uniformly Porous Slit with Porous Medium: an Application to the Diseased Renal Tubules, *Chinese Journal of Physics*, 2020, 64, 264-277.
[17] Almuthaybiri, S. S. and Tisdell, C. C., Laminar Flow in Channels with Porous Walls: Advancing the Existence, Uniqueness and Approximation of Solutions via Fixed Point Approaches, *Journal of Fixed Point Theory and Applications*, 2022, 24(3), 1-21.
[18] Jha, B. K. and Yusuf, T. S., Transient Dean Flow in a Composite Annular Duct with Porous Walls Partially Filled with Porous Material, *Propulsion and Power Research*, 2022, 11(1), 118-128.
[19] Berman, A. S., Laminar Flow in Channels with Porous Walls, *Journal of Applied Physics*, 1953, 24(9), 1232-1235.

[20] Tilton, N. and Cortelezzi, L., Linear Stability Analysis of Pressure-Driven Flows in Channels with Porous Walls, *Journal of Fluid Mechanics*, 2008, 604, 411-445.

[21] Casalis, G., Avalon, G. and Pineau, J.-P., Spatial Instability of Planar Channel Flow with Fluid Injection through Porous Walls, *Physics of Fluids*, 1998, 10(10), 2558-2568.

[22] Deng, C. and Martinez, D. M., Linear Stability of a Berman Flow in a Channel Partially Filled with a Porous Medium, Physics of Fluids, 2005, 17(2), 024102.

[23] Hona, J., Modeling of Heat and High Viscous Fluid Distributions with Variable Viscosity in a Permeable Channel, *International Journal of Multiphysics*, 2015, 9(4), 341-360.

[24] Nyemb N. V. and Hona, J., Modeling and Simulation of Suction-Driven Flow and Heat Transfer with Temperature-Dependent Thermal Conductivity in a Porous Channel, *International Journal of Thermofluid Science and Technology*, 2022, 9(3), 090303.

[25] Pom, G. K., Hona, J., Nyemb, N. V. and Nganbe II, M. M., On the Behavior of the Flow Field Components from the Momentum Equation for a Functioning Model of Rocket Motors, *International Journal of Thermofluid Science and Technology*, 2022, 9(4), 090402.

[26] Lehel, F. R. P. and Hona, J., Similarity Solutions of the Navier-Stokes Equations for an Injection-Driven Flow Between Two Orthogonally Moving Porous Discs, *Chinese Journal of Physics*, 2021,73, 360-374.

[27] Nganbe II, M. M., Hona, J., Ngo Nyobe, E. and Pemha, E., Circular Flow Around a Turning Point in an Annular Area Between Two Coaxial Porous Cylinders, *The European Physical Journal Plus*, 2019, 134(5), 236.

[28] Zaturska, M. B., Drazin, P. G. and Banks, W. H. H., On the Flow of a Viscous Fluid Driven Along a Channel by Suction at Porous Walls, *Fluid Dynamics Research*, 1988, 4(3), 151-178.

[29] Cox, S. M., Two-Dimensional Flow of a Viscous Fluid in a Channel with Porous Walls, *Journal of Fluid Mechanics*, 1991, 227, 1-33.

[30] Dauenhauer, E. C. and Majdalani, J., Exact Self-Similarity Solution of the Navier-Stokes Equations for a Porous Channel with Orthogonally Moving Walls, *Physics of Fluids*, 2003, 15(6), 1485-1495.

[31] Terrill, R. M., Laminar Flow in a Uniformly Porous Channel, *Aeronautical Quarterly*, 1964, 15(3), 299-310.

[32] Sellars, J. R., Laminar Flow in Channels with Porous Walls at High Suction Reynolds Number, *Journal of Applied Physics*, 1955, 26, 489-490.